Peer-reviewed version available at Metals 2018, 8, 584; doi:10.3390/met8080584

Article

Research on Influential Mechanism of HAZ Impact Toughness for Ship-building Steel with Mg Addition

Hui-rong Li [1], Li-gen Sun[1,*], Li-guang Zhu[1], Yun-song Liu[1], Yun-gang Li[1]

[1] College of Metallurgy and Energy, North China University of Science and Technology-NSCT
* Correspondence: sunligen1983@outlook.com; Tel.: +86-13315568791

Abstract: The welding performance of shipbuilding steel under large heat input could be improved greatly by the Mg addition to the steel, but the impact toughness of the HAZ is not stable. According to the three different thickness steel plates obtained in the industrial experiment, the large heat input welding was carried out by different heat input, and the impact toughness analysis, impact fracture analysis, metallographic microstructure analysis and inclusions analysis were carried out. The results showed that, the HAZ of three kinds of thickness plates induced a lot of IAF, with Mg addition, the inclusion dimension had been reduced effectively, and the IAF induced ability of the inclusions had also been improved. The difference of HAZ impact toughness with different welding heat input and different impact temperature is significant, in consideration of the influence of welding heat input and metallographic microstructure on impact toughness of HAZ, the welding heat load had far greater effect than metallographic microstructure on ductile-brittle transition temperature. At the same time, if the original metallographic microstructure of steel was coarse, the pinning effect of the inclusions would be reduced significantly, and the microstructure of HAZ would be coarsened and the impact toughness of HAZ would be decreased, so there is a certain matching relationship between the metallographic microstructure and the inclusion dimension.

Keywords: oxide metallurgy; impact toughness; metallographic structure; inclusion; ductile-brittle transition temperature

1. Introduction

In recent years, the shipbuilding industry has developed rapidly, especially in eastern Asia. In order to further shorten the shipbuilding time and improve competitive power, high-efficiency large heat input welding technology has been brought into. The upgrade of welding technology put forward new requirements for the ship structural steel, that is, the shipbuilding steel should have higher strength and higher toughness, and must also have good high heat input weldability. The so-called high heat input welding refers to the welding line energy ≥ 50kJ/cm, and it is efficient welding method. Under the high input energy of the welding line, the traditional HAZ (heat affect zone) of the shipbuilding steel would undergo severe grain coarsening, localized softening and embrittlement, and resulted in a significant reduction in impact toughness and a serious threat to the safety of the ship structure.

In order to improve the impact toughness of the HAZ, J. Takamura and S. Mizoguchi [1-2] worked in Nippon Steel proposed the application of oxide metallurgy technology to the development of shipbuilding steel for high heat input welding for the first time. According to J. Takamura and S. Mizoguchi, a large number of finely dispersed inclusions in the steel pinned prior austenite grains to prevent their growth; on the other hand, they could induce IAF (intragranular acicular ferrite), and further refines the intragranular structure. Around this type of inclusions with double grain refinement effect, especially the ability to induce IAF, many scholars had carried out a lot of research work. Hitoshi H [3] and Shu Wei [4] found that TiOx and MnS composite inclusions can effectively induce the IAF, and the size of such inclusions is generally less than 3μm [5].

However, the induction effect of TiOx is not stable, because it tends to agglomerate and grow, and is difficult to realize distribution diffusely, the coarse TiOx inclusions could also be the source of steel cracks. Vega M I [6] and S. Kanazawa [7] believed that TiN could effectively induce IAF and was not easily condensed. However, Kasamatsu Y [8] found that when the temperature exceeds 1350℃, TiN would partially solid-solubilize, the amount of TiN will drop sharply after cooling and precipitation then, and leaded to a significant decrease in its inducing ability. Therefore, this method limits the input line energy during welding. In order to obtain dispersed and stable Ti-containing inclusions, scholars began to add microalloying elements such as Mg (Ca) to the steel [9-11]. At present, the development of this Mg-based shipbuilding steel is at the forefront of the research and application of oxide metallurgy theory and technology.

As the representative parameters of comprehensive mechanical properties of shipbuilding steel, impact toughness influence factors include steel composition, rolling process, heat treatment process, metallurgical composition and impact test temperature [12-15]. For the heat affected zone of Mg-based shipbuilding steel involved in this study, the main influencing factors are the grain coarsening caused by welding heat load and the corresponding impact test temperature.

In this study, corresponding large heat input welding and impact tests at different temperatures were carried out for steel plates with different thicknesses. At the same time, the morphology of the impact fractures, microstructures, and the presence of inclusions were systematically studied, to obtain of the impact toughness influence mechanism of HAZ for Mg-based shipbuilding steel, an effective way to improve the energy weldability of shipbuilding steel would also be explored.

2. Materials and Methods

The Mg-based shipbuilding steels used in the experiments were trial-produced in a real steel plant. The chemical composition is shown in Table 1. For the rolling process, TMCP technology had been used, and the slabs were rolled into three thickness plates of 16mm, 25mm and 40mm, respectively, and the three types of steel plates were from the same heat. The initial rolling temperature was 1050-1120℃, and the final rolling temperature was controlled at 890-830℃. The yield strengths of the three-thickness steel plates all exceeded 460 MPa, and the tensile strengths exceeded 520 MPA, the elongations of 40 mm-thick steel plate exceeded 23%, and for the other two exceeded 32% , the cold bending performance of the three was also up to standard. For impact work at -20℃, three thicknesses of steel plate exceeded 230J, and 25mm thick steel plate exceeded 300J, which greatly exceeded the requirements of classification society (CCS) for EH36 plate steel.

Table.1 The chemical composition of the steel trial (mass%).

Composition	C	Si	Mn	S	P	Al	Ti	Mo	V	Nb	Mg
content	0.08	0.20	1.40	0.005	0.015	0.01	0.015	0.07	0.04	0.04	0.005

For large heat input welding technique, the thicker the steel base material, the higher the required welding line energy. In order to ensure that the steel plates was welded together and the melting of the steel plate caused by excessive line energy is avoided at the same time, various input line energies had been tested for the three thickness steel plates, and the final determination was that, the 16 mm thick steel plate adopted 50 kJ/cm input line energy, 25mm thick steel plate adopted 100kJ/cm input line energy, 40mm thick steel plate adopted 150kJ/cm l input line energy. The specific welding parameters and wire material are shown in Table 2, in which the 16mm thick steel plates were welded by monofilament submerged arc welding, and the 25 and 40mm thick steel plates were welded by double wire submerged arc welding. The welding method is flat V-groove butt welding.

After the welding, the impact specimen had been prepared by wire cut. For each plate, according to GB/T 229-2007, the position 2 mm that from the fusion line was selected to been tested for the impact toughness of the weld heat affected zone. The impact temperatures were -20℃ and -40℃. Three test specimens were selected for impact test at each test temperature. The final results were averaged, and the total number of test specimens was 18.

Table.2 Welding parameters

Thickness (mm)	input line energy (KJ/cm)	Welding speed (m/h)	welding wire diameter (mm)	welding wire kinds	fore wire current (A)	fore wire voltage (V)	hind wire current (A)	hind wire voltage (V)
16	50	19.6	4.0	10Mn2	780	35		
25	100	24	5.0+5.0	10Mn2+SJ501	1000	41	700	37
40	150	22.7	5.0+5.0	10Mn2+SJ501	1200	44	1000	42

After the impact test, the fracture surface morphology, metallographic structure and inclusions of the impact specimen were analyzed by using stereomicroscope, optical microscope, scanning electron microscope and energy spectrum.

3. Results

3.1. Impact testing

Table 3 shows the results of impact toughness of the welding heat affected zone with different thicknesses at -20℃ and -40℃.

Tab.3 Impact results

thickness /mm	input line energy /kJ/cm	impact temperature/ ℃	impact absorbed energy /J			Averaged value /J
16	50	-20	197.3	166.7	172.0	178.7
		-40	89.6	49.0	74.3	71.0
25	100	-20	42.5	91.4	38.6	57.5
		-40	51.8	30.2	17.4	33.1
40	150	-20	198.9	189.5	197.6	195.3
		-40	32.9	35.7	27.5	32.0

From the test results in Table 3, it shows that, at -20℃, 16mm thickness steel plate and 40mm thickness steel plate had better impact toughness values in the heat-affected zone under the corresponding high heat input welding conditions, especially for 40mm thickness steel plate. The average impact energy had reached 195.3J; while the 25mm steel plate under 100kJ/cm line energy welding, the corresponding average impact energy value is only 57.5J, which is relatively low.

When the test temperature is lowered from -20 ℃ to -40 ℃, the impact energy values of the three were greatly reduced, the impact energy value of HAZ for the 16mm thickness steel plate is 71J, and the 25mm and 40mm were only 33.1J and 32J, respectively. Although the values had reached the national standard requirements, but were very low.

3.2. Impact fracture

3.2.1. Macroscopic feature

The macroscopic fracture morphologies of impact fracture for different thickness at different temperatures were observed under a 50-fold microscope, and the typical morphology of impact fractures at -20℃ are shown in Figure1, the typical morphology of impact fractures at -40℃ are shown in Figure2.

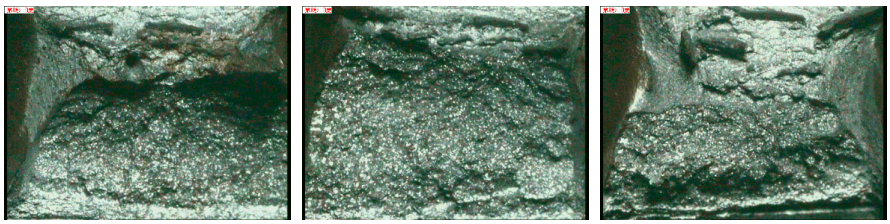

（a）16mm （b）25mm （c）40mm

Figure 1. Macroscopic fracture (-20℃)

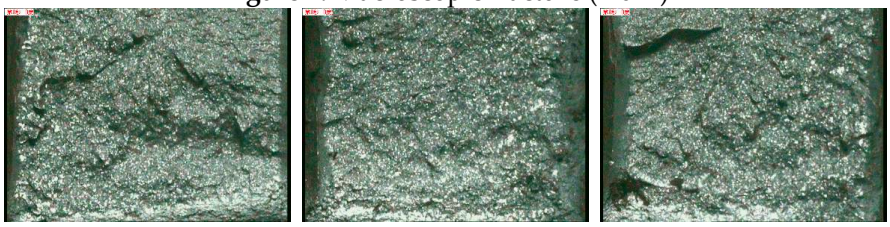

（a）16mm （b）25mm （c）40mm

Figure 2. Macroscopic fracture (-40℃)

As shown in Figure1 and Figure2, the impact section structures of the HAZ for the three-thickness steel plate at -20℃ were much better than these at -40℃. At -20℃, the common feature of the three typical impact fractures was that the impact specimen has a large number of deep elongated shear lips near the narrow part of the V-groove area [17], and it appeared farther away from the impact V-groove, obvious fibrous, fractured areas were filled with relatively sharp tear edges, which indicating that the impact toughness of the HAZ is better at -20℃. For comparison, the ratio of the long shear lip in the fracture of the 25mm steel plate was relatively low, and the impact absorbed energy was also significantly lower than the other two.

Compared with above, the three typical impact fractures in Figure 2(a), 2(b), and 2(c) were relatively flat, with a large number of small facets, radial and herringbone stripes, and there was no obvious tearing edge.

3.2.2 Microscopic feature

The impact fracture specimen was sampled by wire cut at a distance of 10 mm from the fracture surface. The sample was cleaned with an ultrasonic cleaner, then wiped with alcohol, dried, and finally placed in a scanning electron microscope to observe the microscopic appearance of the fracture. The typical microscopic morphology of impact fractures for different plate thicknesses at -20℃ are shown in Figure 3, and the typical microscopic morphology of impact fractures for different plate thicknesses at -40℃ are shown in Figure 4.

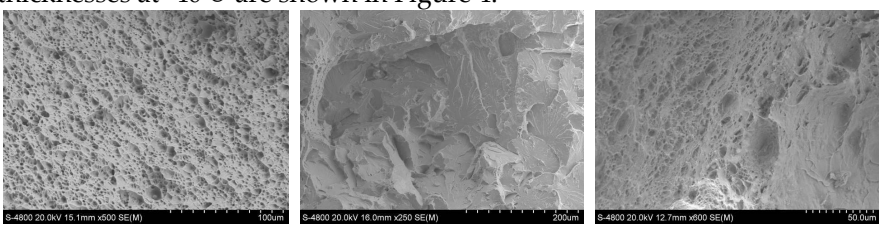

（a）16mm （b）25mm （c）40mm

Figure 3. Sample micro-fracture(-20℃)

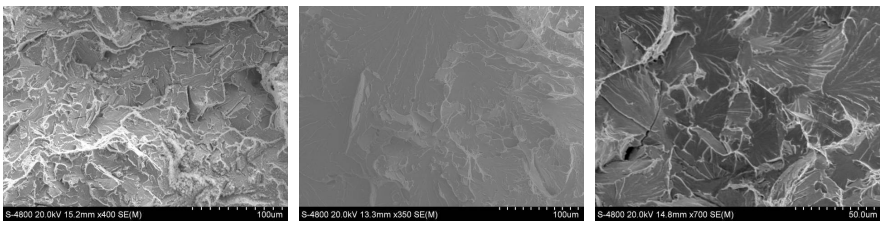

（a）16mm （b）25mm （c）40mm

Figure 4. Sample micro-fracture(-40℃)

Peer-reviewed version available at Metals 2018, 8, 584; doi:10.3390/met8080584

Typical micrographs of impact fractures in the heat affected zone of steel plates thickness 16mm, 25mm, and 40mm at -20℃ are shown in Figure 3(a), 3(b), and 3(c), and the impact absorbed values were 197.3J, 42.5J, and 197.6J, respectively. Among them, the fracture micro-morphology shown in Figure 3(a) was a dense and unequal equiaxed dimple formed by tensile pulling force, and there was a phenomenon of enrichment of small dimples near the large dimple, and it was the typical ductile fractures; as shown in Figure 3(b), the microscopic morphology of the fractures was as a fan-shaped cleavage pattern, in which there were distinct torn edges, and there were very few small and shallow dimples in some regions, and there were also solutions in the entire section. Columns are typical quasi-cleavage fractures; the fractures shown in Figure 3(c) were composed of sheared elongated dimples and partially shallow and small equiaxed dimples, in which elongated dimples had a certain direction. The reason for the above is that the sample was punctured and ruptured under the impact of an impact force and was a typical ductile fracture. For the perspective of the fracture mechanism, the microscopic morphologies of the three types of fractures were consistent with the corresponding impact energy values [16-18].

As shown in Figure 4, 4(a), 4(b) and 4(c) are the typical microscopic appearances of impact fractures in the HAZ of steel plate thicknesses of 16mm, 25mm and 40mm at -40℃, respectively, under the corresponding energy welding conditions. The corresponding impact absorbed values were 49.0J, 17.4J and 35.7J, respectively. Among them, Figure 4(a) shows that, the uneven dimples appeared in the micro-morphology of the fracture surface, there were also some smaller cleavage surfaces, and clearer tearing edges, which were typical characters of the quasi-cleavage fracture; Figure 4(b) shows that, the micro-morphology of the fracture was mainly a river pattern. During the process of extending from the cleavage crack outward to the crystal phase, a large number of steps gather and the direction of the river flow were consistent with the direction in which the crack extends outward. The brittle fractures of Figure 4(c) shows fracture features resembling “fans” at the fractures, which were mainly due to cleavage cracks originating in the crystal near the grain boundary, and the river pattern would be in the form of a fan to extend outwards, and these were the typical quasi-cleavage fracture [16-18].

As shown in the experimental results, it can be seen that both the macroscopic appearance and the microscopic appearance of the fracture were matched with the corresponding impact absorbed energy values, and there was no sharp drop in the impact absorbed energy value caused by the steel plate defect, which indicated that the impact energy value could be completely represents the impact toughness of the HAZ of the steel plate under the corresponding welding and impact conditions.

4. Discussion

4.1 Influence of welding heat input

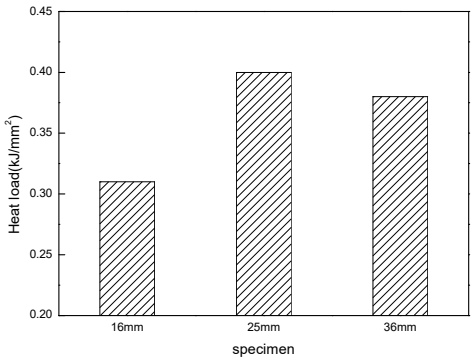

Figure 5. Welding heat load

For normal conditions, the welding line energy characterizes the heat input per welding area, but for different thickness steel plates, the heat load in the local area does not necessarily increase with the increase of weld heat input, it also depends on the steel plate thickness. For this reason, the

186 welding heat load of three kinds of steel plates had been calculated. The results are shown in Figure
187 5. From Figure 5, it could be seen that the 25mm thickness steel plate had the highest heat load,
188 reached 0.40kJ/mm^2, which would exacerbate the tendency to deteriorate the microstructure of the
189 heat-affected zone, which may be one of the causes for its lower impact toughness. Although the
190 thermal load of the 40mm thickness steel plate has reached 0.38kJ/mm^2, the impact on the impact test
191 results was relatively small.
192 At -40℃, the impact absorbed energy values of the three were greatly reduced, especially for
193 the 40mm thickness steel plate, which corresponding impact energy value reduced 163.3J, even
194 lower than the corresponding value of the 25mm thickness steel plate which is 32.0J. The impact
195 energy value of the 16mm thickness steel plate is 71J, more than twice that of the other two. The key
196 factor that causes this result was the ductile-brittle transition temperature of the test steel.
197 The ductile-brittle transition temperature of steel is influenced by factors such as thermal
198 processing [19-20], metallurgical composition [21], and grain boundary precipitation [22]. For this
199 research, the metallographic structure properties and heat load were closely related in welding
200 process [23]. From Figure 5, it could be seen that the corresponding heat load of the 16mm thickness
201 steel plate was significantly lower than the other two, and the impact energy value at the -40℃
202 corresponding to the HAZ is 71J, which was obviously higher than that of the other two also. It is
203 shown that, the welding heat input had a great influence on the ductile-brittle transition temperature
204 of the steel.
205 In theory, the cooling rate has a greater impact on the microstructure [24-25]. With the increase
206 of the thickness of the steel plate, under the same external cooling conditions, the greater the
207 thickness of the steel plate, the lower the overall cooling rate. Moreover, the heat loads of 25mm and
208 40mm thickness steel plates were all higher than those of 16mm, so the impact of welding heat input
209 on impact toughness of 25mm and 40mm thick steel plates, especially the impact on the
210 ductile-brittle transition temperature, was significantly higher than that of 16mm thick steel plates.
211 However, at the same time, at -20℃, without considering of the influence of the ductile-brittle
212 transition temperature of the test steel, the impact toughness of 40mm thickness steel plate was
213 much higher than that of 25mm, so the metallographic structures of the three thickness steel plates
214 should be analyzed further.

215 *4.2 Analysis of metallographic structures*

216 The metallographic structure of 16 mm thickness steel plate with welding heat input 50 kJ/cm
217 under 200-fold field of view are shown in Figure 6. Figure 6(a) is the welding fusion zone, Figure
218 6(b) and 6(c) are the welding heat affected zone, and Figure 6(d) is the metallographic structure of
219 the steel plate.

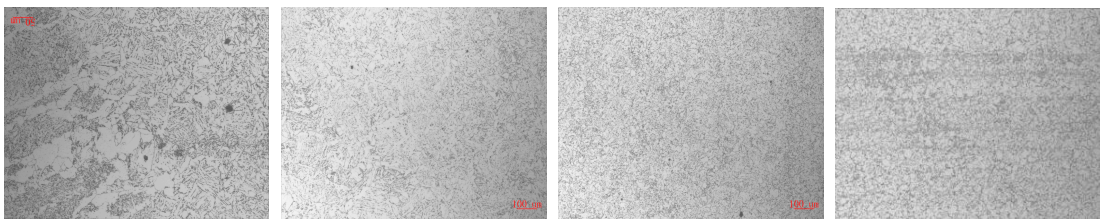

220

221 (a) welding fusion zone (b)HAZ-1 (c)HAZ-2 (d) steel plate

222 **Figure 6.** Metallographic structure of HAZ for 16 mm thickness (200×)

223 As shown in Figure 6(a), the metallographic structure of the HAZ in the right half of the weld
224 line was a little thicker, which was approximately 100 μm away from the weld line, but with the
225 distance increasing, the structure became finer. Combining with the metallographic structures of the
226 two welding heat affected zones in Figure 6(b) and 6(c), it could be found that the overall HAZ
227 structure was relatively uniform, and due to the appearance of a large number of IAF, The austenite
228 grain in the heat-affected zone had been effectively fined. For the entire weld heat affected zone, the

nearer to the weld line, the higher the rate of IAF in the metallurgical structure. Under the condition that a large number of IAF were induced, the heat affected zone was even more fine and uniform than the original plate (as shown in Figure 6(d)).

The metallographic structure of 25 mm thickness steel plate with welding heat input 100 kJ/cm under 200-fold field of view are shown in Figure 7. Figure 7(a) is the welding fusion zone, Figure 7(b) and 7(c) are the welding heat affected zone, and Figure 7(d) is the metallographic structure of the steel plate.

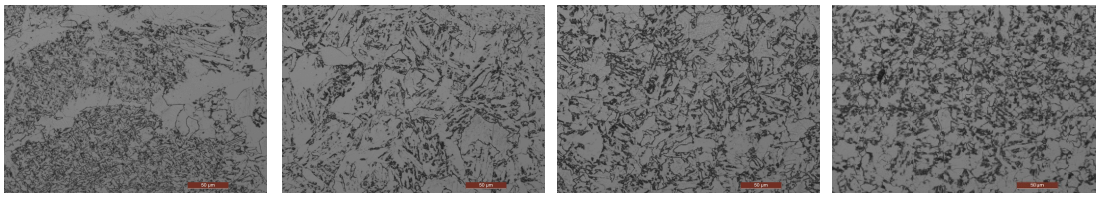

(a) welding fusion zone (b)HAZ-1 (c)HAZ-2 (d) steel plate

Figure 7. Metallographic structure of HAZ for 25mm thickness (200×)

As shown in Figure 7(a), the metallographic structure of the right side of the fusion line was significantly coarsened. The metallographic structure of the HAZ showed in Figure 7(b) was closer to the weld fusion line, it is shown that, the metallographic structure in the lower left area was significantly coarser than that in the upper right area, and the microstructure in the upper right area was same to metallographic the structure shown in Figure 7(c). This showed that, due to the larger heat load of the 25 mm thickness steel plate, it metallographic structure was coarsened obviously. However, due to the induction of IAF, which had effectively restricted the coarsening of the microstructure, the roughening of the most of the heat-affected zones was not serious compared with the steel plate. This is the reason that its impact toughness value of the 25mm thickness steel plate could reach twice of the national standard.

The metallographic structure of 40 mm thickness steel plate with welding heat input 150 kJ/cm under 200-fold field of view are shown in Figure 8. Figure 8(a) is the welding fusion zone, Figure 8(b) and 8(c) are the welding heat affected zone, and Figure 8(d) is the metallographic structure of the steel plate.

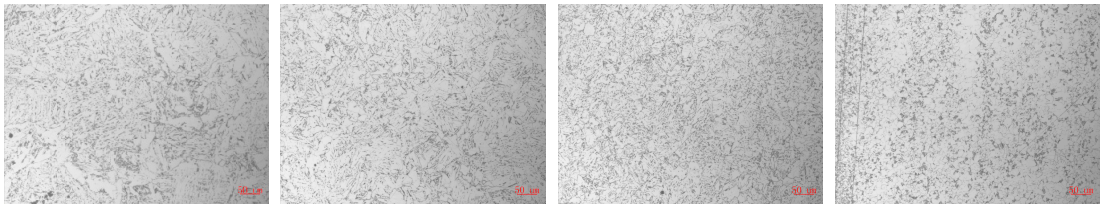

(a) (b) (c) (d)

Figure 8. Metallographic structure of HAZ for 40 mm thickness (200×)

At -20℃, the HAZ impact toughness of 40mm thickness steel plate was similar to 16mm thickness steel plate, as shown in Figure 8(a), 8(b), 8(c), and 8(d), the metallographic structure was also as same as the corresponding area of the 16mm thickness steel plate. With a large amount of IAF inducing, the metallographic structure of HAZ was not only no coarser, but also even more uniform and finer than steel plate.

For above analysis, it could be seen that the welding heat load of a 25 mm thickness steel plate was not much different from 40 mm thickness steel plate, but the impact toughness value was significantly lower than 40 mm thickness steel plate. As shown in Figure 7(d) and 8(d), the microstructures of 25 mm thickness steel plate was significantly thicker than the 40 mm thickness steel plate, and the corresponding welded heat affected zone were also showed the same

phenomenon. Due to the coarseness of the original structure of the steel plate, the microstructure of the welding heat affected zone is severely roughened, which indicates that the resistance of the coarse structure to the weld line energy is far worse than that of the fine structure. This also leads to the reduction of the impact toughness of the welded heat affected zone of the 25 mm thickness steel plate. The above analysis indicates that the TMCP process used to roll 25 mm thick steel plates in actual production needs further optimization.

At -40℃, the metallographic structure of the weld heat affected zone does not change, but the corresponding impact toughness value of the 40mm thickness steel plate decreases drastically, that indicated that the ductile brittle transition temperature of the test steel was not directly related to the thickness of the metallographic structure. Shen Dongdong etal [26] have also obtained similar results.

Through the above metallographic analysis, it could be found that the metallographic structure of the HAZ of the 16mm and 40mm thickness steel plates was even finer than that of the original steel plate. The HAZ metallographic structure of the 25mm thickness steel plate was coarser than the original steel plate. That was attributed to the induction of the amount of IAF in the HAZ. Therefore, it is necessary to do further analyze about the inclusions which induced the IAF.

4.3Analysis of inclusions

For oxide metallurgical steels, the inclusions could pin the austenite grains to prevent the growing, and could also induce the IAF in the austenite grains to make the grain finer. Therefore, for the HAZ with the three different thicknesses steel plates, the number of micro-inclusions had been statistically graded in this study [27-28], and the results are shown in Table 4.

Table 4. Statistical result of micro-inclusions in different HAZ

thickness of steel plate	0-5μm	5-10μm	10-15μm	15-20μm
16mm	83	14	16	14
25mm	100	20	8	2
40mm	67	26	6	10

As shown in Table 4, the inclusion size of the HAZ was mainly in the range of 0-5μm. These types of oxides could be nuclear core for IAF inducing and play the pinning effect to restrict austenite grains growing. In comparison, for the range of 0-5μm, the maximum number of inclusions in the heat affected zone of the 25 mm thick steel plate was the largest, but the IAF rate of the 25mm thickness steel plate was relatively low, this may be due to the relative thicker metallographic structure for the 25mm thickness original steel plate.

The oxide metallurgy effect for the different size inclusions is closely related to the metallographic structure of the steel plate. From the previous studies of the authors, in the as-cast condition, the IAF had been induced by the inclusions mainly with the size of 10 μm, and inclusions in the range of 15-20 μm could also be used as the core to induce the IAF, but for the rolled plate with smaller grain size, the IAF could only be induced by the smaller inclusions.

The typical morphologies of IAF and its inducing cores (inclusions) were shown in Figure 9. It is shown that, these inclusions were substantially spherical and their size were mostly about 3 μm. In order to further analyze the composition of inclusions, in this study, scanning electron microscopy and energy spectroscopy were used to perform surface scan analysis of inclusions. The representative inclusion surface scans are shown in Figures 10 and 11, respectively. In this study, the five elements of Mg, Al, Mn, Ti and S that have an important influence on the induction of IAF were mainly investigated.

Peer-reviewed version available at Metals 2018, 8, 584; doi:10.3390/met8080584

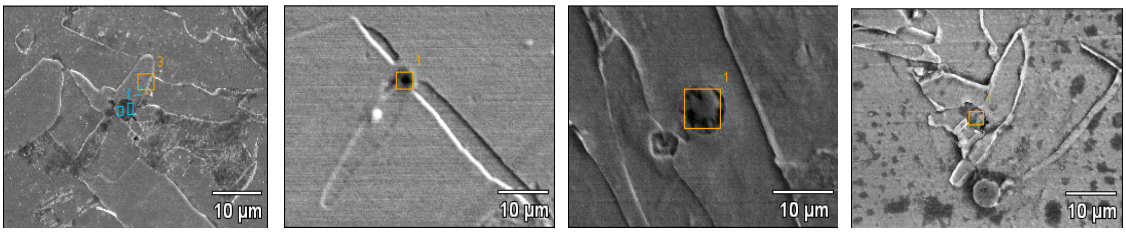

(a) (b) (c) (d)

Figure 9. Typical characters of the inclusions which induced IAF

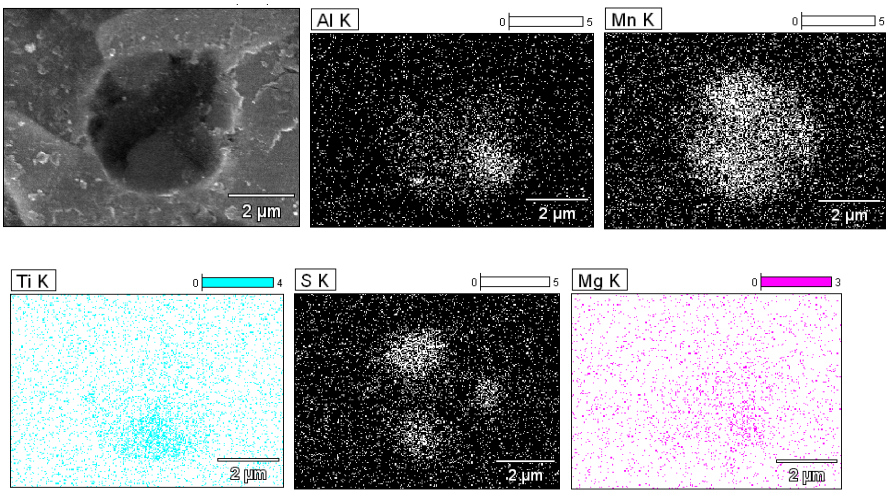

Figure 10. Surface scanning analysis of inclusions that contain Mg

Figure 10 is a typical surface scan of Mg-containing inclusions that induced IAF. As shown in Figure 10, the size of the inclusion was 3-4μm, corresponding to the inclusion in Figure 9(b). For the five elements examined, the Mg elements basically diffusely distributed; the Mn element was substantially full of inclusions, but was more concentrated at three positions; the Al and Ti elements were relatively more concentrated in the lower half; the S elements were concentrated in inclusions three points on the periphery.

As shown in Figure 9(b), the inclusions induced a total of three acicular ferrite branches, and the three branches correspond to the three points in S. Under normal conditions, S existed in the form of MnS, and the concentration of S and Mn causes the decrease of the Mn content in the surrounding area, which in turn induces acicular ferrite.

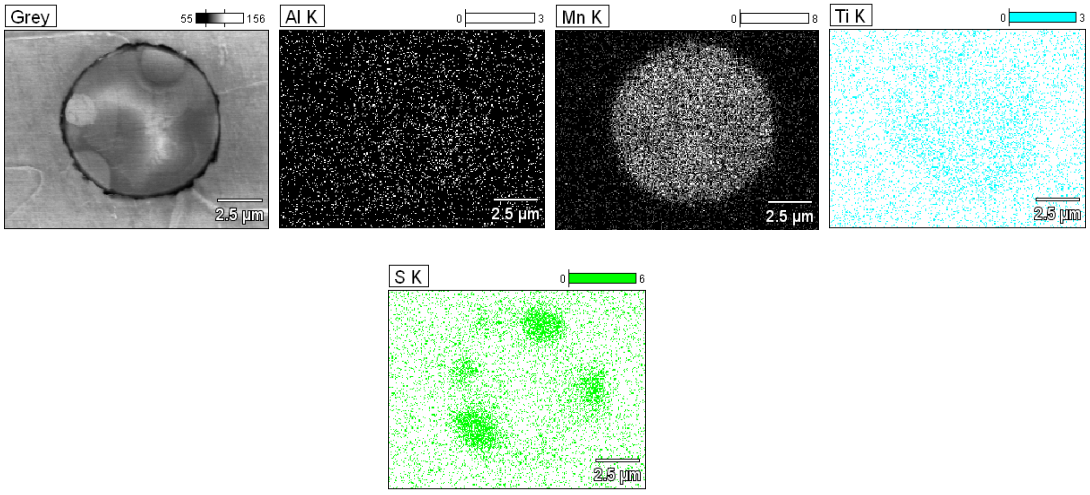

Figure 11. Surface scanning analysis of inclusions that free from Mg

Figure 11 is a typical surface scan of Mg-free inclusion that induced IAF. As shown in Figure 11, the size of the inclusion was about 7μm, corresponding to the inclusion in Figure 9(c). Among the elements examined, the Mn element was substantially filled with the entire inclusion; Al and Ti elements were basically dispersed; S element was concentrated on the four points of the periphery of the inclusion and appeared in the other two areas on the periphery of the inclusion.

As shown in Figure 9(c), the inclusion was within an elongated IAF, whose width exceeding 10μm. Although it also induceed acicular ferrite, due to the relative thickness of the tissue, its performance should be inferior to that of the IAF induced by the inclusions shown in Figure10.

From the comparison of Figure 10 and Figure 11, it could be found that although Mg element is not the primary cause for the IAF inducing, but Mg can effectively reduce the size of inclusions, and thus increase the inclusion ability of IAF inducing, so for the steel in this research, Mg is essential.

5. Conclusions

(1) The HAZ of three kinds of thickness plates induced a lot of IAF, with Mg addition, the inclusion dimension had been reduced effectively, and the IAF induced ability of the inclusions had also been improved. if the original metallographic microstructure of steel was coarse, the pinning effect of the inclusions would be reduced significantly, and the microstructure of HAZ would be coarsened and the impact toughness of HAZ would be decreased, so there is a certain matching relationship between the metallographic microstructure and the inclusion dimension.

(2)Mg is not the primary cause of the IAF inducing, but Mg can effectively reduce the size of inclusions, and thus increase the inclusion ability of IAF inducing.

(3) The difference of HAZ impact toughness with different welding heat input and different impact temperature is significant, in consideration of the influence of welding heat input and metallographic microstructure on impact toughness of HAZ, the welding heat load had far greater effect than metallographic microstructure on ductile-brittle transition temperature.

Author Contributions: Conceptualization, Li-gen Sun; Funding acquisition, Li-guang Zhu and Li-gen Sun; Software, Yun-song Liu; Supervision, Yun-gang Li and Li-gen Sun; Writing – review & editing, Hui-rong Li.

Funding: This research was funded by National Natural Science Foundation of China, grant number 51474089, and by Natural Science Foundation of Hebei Province, grant number E2017209194.

Acknowledgments: We would like to extend my sincere gratitude to Professor Wang Shuoming and Professor Liu Zengxun, for their instructive advice and useful suggestions on the thesis. We also thanks the engineers in Handan steel company, they provided a lot for the industrial experiment.

Conflicts of Interest: The authors declare no conflict of interest.

References

1. J. Takamura, S. Mizoguchi. Role of oxides in steels perform ances metallurgy of oxides in steels. ISIJ Proceedings of the sixth international iron and steel congress, Nagoya, ISIJ，1990: 591-597.
2. S. Mizoguchi and J. Takamura. Control of oxides as inoculants metallurgy of oxides in steels. Proceedings of the sixth international iron and steel congress, Nagoya, ISIJ,1990: 598-604.
3. Hitoshi H. Effect of Ti and alloying elements on microstructure and toughness of simulated HAZ of 780 MPa class steels. Tetsu-to-Hagane, 2004, 90(5): 271-277.
4. Shu Wei, Wang Xuemin, Li Shurui, et al. Nucleation and growth of intragranular acicular ferrite and its effect on grain refinement of the heat-affected-zone. Acta Metallurgica Sinica, 2011, 47(4): 435-441
5. Hong S G, Kang K J, Park C G. Strain-induced precipitation of NbC in Nb and Nb-Ti microalloyed HSLA steels. Scrita Materialia, 2002, 46(2): 163-168.
6. Vega M I, Medina S F, nfluence of TiN particle precipitation state on static recrystallisation in structural steels. ISIJ International，2005，45(12) : 1878-1886.
7. S. Kanazawa, A. Nakashima, K. Okamoto, et al. Improved toughness of weld fussion zone by fine TiN particles and development of a steel for large heat input welding. Tetsu-to-Hagane, 1975, 61(11): 2589-2603.

8. Kasamatsu Y. Effect of titanium and nitrogen on toughness of heat-affected zone of steel plate with tensile strength of 50kg /mm² in high heat input welding. Tetsu-to-Hagane, 1979，65(8) : 1232-1241.
9. Song Mingming, Song Bo, Hu Chunlin, et al. Effect of Ti--Mg complex deoxidation on the microstructure and impact properties of HAZ in steel. Chinese Journal of Engineering, 2015, 37(7): 883-888.
10. Kai Zhu, Zhenguo Yang. Effect of Mg addition on the ferrite grain boundaries misorientation in HAZ of low carbon steel. Journal of Materials Science and Technology, 2011, 27(3): 252-256.
11. Sun Zhan, Huang Jihua, Zhang Hua, et al. Microstructures and mechanical properties of joints of mi-croalloyed EH40 ship steel with high heat-input welding. Transactions of the China Welding Institution, 2008, 29(3): 42-43.
12. Seok Su Sohn, Seokmin Hong, Junghoon Lee, Byeong-Chan Suh, Sung-Kyu Kim, Byeong-Joo Lee, Nack J. Kim, Sunghak Lee. Effects of Mn and Al contents on cryogenic-temperature tensile and Charpy impact properties in four austenitic high-Mn steels. Acta Materialia, 2015, 100: 39-52.
13. Byoungchul Hwang, Chang Gil Lee. Influence of thermomechanical processing and heat treatments on tensile and Charpy impact properties of B and Cu bearing high-strength low-alloy steels. Materials Science and Engineering A, 2010, 527: 4341-4346
14. You Yang, Wang Xuemin, Shang Chengjia. Influence of austenitizing temperature on the microstructure and impact toughness of a high strength low alloy HLSA100 steel. Acta Metallurgica Sinica, 2012, 48(11): 1290-1298.
15. Hyo Kyung Sung, Sang Yong Shin, Wooyeol Cha, Kyungshik Oh, Sunghak Lee, Nack J. Kim. Effects of acicular ferrite on charpy impact properties in heat affected zones of oxide-containing API X80 linepipe steels. Materials Science and Engineering A, 2011, 528: 3350-3357.
16. Li Liang, Cao Feng, Wang Yalong, Zhang Xiang, Lu Caihong. Analysis on low temperature impact toughness and fracture morphologies of X90 pipeline steel. Heat Treatment of Metals, 2015, 40(1):190-193.
17. Pan Tao, Hao Yu, Yongfei Fan, Yu Fu. Effects of cooling method after intercritical heat treatment on microstructural characteristics and mechanical properties of as-cast high-strength low-alloy steel. Materials and Design, 2014, 54: 914-923.
18. K.Y.Luo, C.Y.Wang, G.F.Sun, C.Y.Cui, J.Sheng, J.Z.Lu. Investigation and microstructural analyses of massive LSP impacts with coverage area on crack initiation location and tensile properties of AM50 magnesium alloy. Materials Science & Engineering A, 2016, 650: 110-118.
19. AryaChatterjee, D.Chakrabarti, A.Moitra, R.Mitra, A.K.Bhaduri. Effect of deformation temperature on the ductile–brittle transition behavior of a modified 9Cr-1Mo steel. Materials Science & Engineering A, 2015, 630:58-70.
20. Xue Bai, SujunWu, Peter K. Liaw. Influence of thermo-mechanical embrittlement processing on microstructure and mechanical behavior of a pressure vessel steel. Materials and Design, 2016, 89: 759-769.
21. Ali Nazari, Amir Ali Milani, Gholamreza Khalaj. Modeling ductile to brittle transition temperature of functionally graded steels by ANFIS. Applied Mathematical Modelling, 2012, 36: 3903-3915.
22. X. M. Chen, S. H. Song, L. Q. Weng, S. J. Liu, K. Wang. Relation of ductile-to-brittle transition temperature to phosphorus grain boundary segregation for a Ti-stabilized interstitial free steel. Materials Science and Engineering A, 2011, 528: 8299- 8304.
23. Sanjeev Kumar, S.K. Nath. Effect of heat input on impact toughness in transition temperatureregion of weld CGHAZ of a HY 85 steel. Journal of Materials Processing Technology, 2016, 236: 216-224.
24. Hiroki Goto, Kenichi Miyazawa, Kohichi Yamaguchi, et al. Effect of cooling rate on oxide precipitation during solidification of low carbon steels. ISIJ International, 1994, 34(5): 414-419.
25. Hiroki Goto, Kenichi Miyazawa, Kazuaki Tanaka. Effect of oxygen Content on size distribution of oxides in steel. ISIJ International, 1995, 35(3): 286-291.
26. Shen Dongdong, Yuan Zexi. Factors influencing the DBTT of 2.25CrMo steel. Journal of Wuhan University of Science and Technology, 2011, 34(6): 410-413.
27. Yang Lingli, Liu Jianhua, Bao Yanping. Researches on X70 cleanliness in refine and continuous casting process. Journal of University of Science and Technology Beijing, 2007, 29(1):97-100.
28. Li Changrong, Bao Yanping, Liu Jianhua. Investigation of reasonable cleanliness for high-grade linepipe steel scale production. Journal of University of Science and Technology Beijing, 2007, 29(suppl.1):10-13.